A&A, 708, A378 (2026)
https://doi.org/10.1051/0004-6361/202347673

Astronomy & Astrophysics

Discovery of planetary-mass binaries in the Lower Centaurus-Crux association

Claudio Cáceres[1,⋆], Dante Minniti[1,2], Andrea Mejías[3], Matías Gómez[1], Javier Alonso-García[4,5], Valentin D. Ivanov[6], Joyce B. Pullen[1], Roberto K. Saito[7], Leigh C. Smith[8], Enrique Solano[9,10], Juan Carlos Beamín[1], Daniela Rojas-Bozza[1], Paolo Soto[1], and Rodrigo Zelada[1]

[1] Instituto de Astrofísica, Departamento de Física y Astronomía, Facultad de Ciencias Exactas, Universidad Andres Bello, Av. Fernández Concha 700, Santiago, Chile
[2] Vatican Observatory, V00120 Vatican City State, Italy
[3] Departamento de Astronomía, Universidad de Chile, Camino El Observatorio 1515, Las Condes, Santiago, Chile
[4] Centro de Astronomía (CITEVA), Universidad de Antofagasta, Av. Angamos 601, Antofagasta, Chile
[5] Millennium Institute of Astrophysics, Nuncio Monseñor Sotero Sanz 100, Of. 104, Providencia, Santiago, Chile
[6] European Southern Observatory, Karl-Schwarszchild Str. 2, D85748, Garching B. Munich, Germany
[7] Departamento de Física, Universidade Federal de Santa Catarina, Trindade 88040-900, Florianópolis, SC, Brazil
[8] Institute of Astronomy, University of Cambridge, Madingley Rd, Cambridge CB3 0HA, UK
[9] Departamento de Astrofísica, Centro de Astrobiología (CSIC-INTA), ESAC Campus, Camino Bajo del Castillo s/n, 28692 Villanueva de la Cañada, Madrid, Spain
[10] Spanish Virtual Observatory, 28692 Villanueva de Cañada, Madrid, Spain

Received 7 August 2023 / Accepted 2 February 2026

ABSTRACT

Context. The recent discovery of free-floating planets (FFPs) in nearby young stellar associations suggests that these objects might be common in the Galaxy. Our search for FFPs in the young Lower Centaurus-Crux (LCC) association using the VISTA Variables in the Vía Láctea VVV and VVVX surveys revealed several candidates with distances $d < 200$ pc.
Aims. The main goal of the paper is to identify binary FFPs among this sample. The presence of such binaries is useful to contrast two different main formation scenarios: the formation in the circumstellar disk of the parent star with subsequent ejection by dynamical interactions and the in situ formation by gravitational collapse of a protostellar cloud.
Methods. We used the *Gaia*, VVV, VVVX, and DECaPS databases to identify pairs of low-mass objects in the LCC association sharing common proper motions. We examined the optical and near-IR color-magnitude and color-color diagrams, and visually confirmed the detections in the available optical and near-IR images.
Results. We find 17 young low-mass binaries in the LCC association, with distances starting from 68 pc and projected separations ranging from 88 to 6742 au. A couple of candidates have additional faint companions that need confirmation to secure them as triple systems. Adopting an age of 17 Myr for the LCC association, we find that 14 of the components are faint enough to have planetary masses.
Conclusions. Our results indicate that binaries represent $\gtrsim$2% of the population of FFPs in the LCC association, and this suggests that their preferred formation mechanism is the gravitational collapse independent of a star. Also, many of the recently discovered FFPs in LCC may be unresolved giant binary planets. The wide range of colors and flux reversals observed suggests that the existence of clouds in their atmospheres is important and points to continuity with the BD populations.

Key words. surveys – planets and satellites: general – binaries: general – brown dwarfs – stars: low-mass

1. Introduction

There are >6000 extrasolar planets known so far, the majority of which orbit around main-sequence stars. Among them, there are also numerous planetary systems with multiple planets, and the hunt for planetary-mass binaries has been ongoing for more than two decades now. For example, Jayawardhana & Ivanov (2006) reported the discovery of a very low-mass binary system in the ρ Ophiuchi (Oph) star-forming region, with individual masses of 17 + 32 $M_{\rm Jup}$[1], that fall in the brown dwarf regime. The first confirmed binary planet is 2MASS J11193254-1137466, a likely member of the TW Hydra association with two components of 3.7 $M_{\rm Jup}$ separated by 3.6 au (Best et al. 2017).

In spite of the substantial progress made on the local census of stars (Reylé et al. 2021), some low-mass objects such as free floating planets[2] (FFPs) may still be missing. This expectation is supported by the discovery of very faint nearby objects in our vicinity (Luhman 2014; Wright et al. 2014). FFPs are also interesting in the astrobiology context. For example, water-rich FFPs may harbor liquid oceans that could provide suitable environments for life (Stevenson 1999). However, FFPs are notoriously hard to find. Microlensing searches have recently discovered a non-negligible number of FFPs, suggesting that there may be

⋆ Corresponding author: cccacere@gmail.com

[1] Note that we use $M_{\rm Jup}$ to represent the mean Jupiter mass, and M_J for the absolute magnitude in the J band.

[2] Considered here as objects with masses below the deuterium-burning limit of 13 $M_{\rm Jup}$ that are not bound to any star.

even more FFPs that bound planets (Sumi et al. 2011; Clanton & Gaudi 2017; Mroz et al. 2017; Gould et al. 2022). Nevertheless, their frequency is still unclear, and the individual microlensing discoveries are extremely difficult to follow up. This important issue will be one of the main goals to pursue with the future Nancy Grace Roman Space Telescope (Penny et al. 2019; Sajadian 2025).

In recent years, several studies have attempted the search for FFPs in nearby stellar associations. For instance, Miret-Roig et al. (2022) report the discovery of 70-170 FFPs in the USco and Oph regions, which represents the nearest young OB association. This is the largest homogeneous sample of FFPs, and they clearly show the path for finding young FFPs, suggesting again that these objects may be very common in our Galaxy. They also argue that the ejection from planetary systems due to dynamical instabilities should be frequent within the first 10 Myr. In a spectroscopic follow-up study, Bouy et al. (2022) report the discovery of a pair of young FFPs in this sample, with a separation of ∼120″ (∼17 400 au). Posterior studies have reported photometric searches with space-based telescopes with some detections of cool brown dwarfs (BDs) and FFPs. For instance, Bouy et al. (2025) report the detection of a dozen FFPs in LDN 1495 with Euclid Early Release Observations. Langeveld et al. (2024) obtained deep JWST data on NGC 1333 to detect six FFPs and one possible BD+planet binary system. Similarly, De Furio et al. (2025) found interestingly that there might be an observational turnover of the initial mass function at ∼12 $M_{\rm Jup}$, after detecting several FFPs in deep JWST data of NGC 2024. Unlike the growing number of FFPs in recent searches, the number of binary systems has remained low. In a preprint, Pearson & McCaughrean (2023) propose the detection of several Jupiter-mass binary systems in the Orion Nebula Cluster (ONC) with JWST that have been challenged by observational (e.g., Luhman et al. 2024; Luhman 2025) and theoretical studies (e.g., Portegies & Hochart 2025; Parker et al. 2025).

Motivated by the works of Miret-Roig et al. (2022) and Bouy et al. (2022), we extended the work of Mejías et al. (2022a,b), who carried out a search of FFPs in the Lower Centaurus-Crux (LCC) association, to look for binary substellar objects in this region. Their catalog contains several dozen candidate FFPs and BDs that were selected using stringent astrometric and photometric criteria based on the optical and near-IR observations from the *Gaia* mission (Gaia Collaboration 2021, 2023), the DECam Plane Survey (DECaPS; Schlafly et al. 2018), and the VISTA Variables in the Vía Láctea survey (VVV; Minniti et al. (2010, 2018), and its extension (VVVX; Saito et al. 2024). VVV and VVVX are two large near-IR photometric surveys that complement each other in covering both the galactic bulge and disk observable from the southern hemisphere. Both surveys present a small overlap that is used to cross-check the accuracy and quality of observations. The pointing accuracy of the surveys is ∼0.1″ and the photometric errors are ΔJ∼0.01 for $11 < J < 16.5$, $\Delta J \sim 0.03$ at $J = 17.5$, $\Delta K_{\rm s} \sim 0.01$ for $11 < K_{\rm s} < 16.5$, and $\Delta K_{\rm s} \sim 0.03$ at $K_{\rm s} = 17.5$. Hereafter, we refer to the joint dataset as the VVV/X survey (cf. Saito et al. 2024). Our work builds upon the photometric and astrometric data of VVV/X (Kurtev et al. 2017; Smith et al. 2018, 2025; Contreras-Ramos et al. 2007; Alonso-García et al. 2018, 2026), which has yielded, for example, the discovery of faint nearby common proper motion (PM) companions (Beamín et al. 2013; Ivanov et al. 2013; Smith et al. 2015), and also faint nearby objects in the solar neighborhood using the VVVX data in combination with *Gaia* (Mejías et al. 2022b).

The LCC association is located at ∼100–150 pc, and it is a prime laboratory to search for young FFPs. Its members have been found to have ages in the range ∼5–20 Myr, with a peak in the age distribution at ∼10 Myr (Pecaut & Mamajek 2016; Goldman et al. 2018; Squicciarini et al. 2022; Ratzenböck et al. 2023), making the low mass objects brighter with respect to their counterparts in older star-forming regions. Indeed, this association has been well studied as an extension of the large nearby Scorpius association complex (de Zeeuw et al. 1999; Pecaut & Mamajek 2016; Goldman et al. 2018; Moolekamp et al. 2019; Luhman & Esplin 2020; Guo et al. 2025; Prisinzano et al. 2022; Ratzenböck et al. 2023). In particular, Bohn et al. (2022) searched for faint wide companions around K-type main-sequence stars in the Sco-Cen association with *Gaia*. They found 110 co-moving companions in their sample, including 20 of them that lie in the BD mass regime. In this paper, we present our complementary search for binary companions to low-mass objects in this nearby association, extending the search to fainter magnitudes. The discovery of giant binary FFPs is important because they are expected to have identical chemical compositions, ages, and distances, and therefore serve to test a wide suite of theoretical models. Section 2 describes the sample selection. Section 3 presents an analysis of the main properties of the sample. Section 4 focuses on the VVVX-FFP-001 system, the first binary FFP that we discovered, as a detailed example. Section 5 gives a summary of other individual targets. In Section 6 we enumerate alternative interpretations to our candidates and discuss some implications of the present findings. Finally, Section 7 presents the conclusions.

2. Data selection results

The southern part of the LCC association is covered by VVV/X, from which we obtained J, H, and $K_{\rm s}$ photometry and astrometry. Complementarily, we obtained *ugrizY* data from DECaPS, and accurate astrometric and photometric data from *Gaia* DR3. We selected candidates on the basis of their parallaxes, proper motions, and locations in the optical and near-IR color-magnitude diagrams (CMDs) and color-color diagrams. First, we bounded the region encompassing LCC in the VVV/X data by considering galactic longitudes in the range $290° \leq l \leq 322°$. The cut in galactic latitudes was set by the limits of the region covered by VVV/X, i.e., $-4.5° \leq b \leq 4.5°$. Within this region, we cross-matched with the DECaPS and *Gaia* catalogs (cf. Smith et al. 2018, 2025; Saito et al. 2024; Mejías et al. 2022c). We selected low-mass objects from these joint datasets by applying the photometric and astrometric selection criteria from Mejías et al. 2022a,c), which minimize the probability of contamination by red-giant stars, and that are based on cuts in IR color indices and the application of the J-magnitude reduced proper motion criteria from Rojas-Ayala et al. (2014). The outcome of this selection is 9118 low-mass candidates.

After this procedure, we applied the following selection parameters, considering quality and kinematical limits for LCC defined by Pecaut & Mamajek (2016); Goldman et al. (2018); Moolekamp et al. (2019); Luhman & Esplin (2020); Prisinzano et al. (2022); Guo et al. (2025): renormalized unit weight error parameter `ruwe` < 1.5, parallax $\varpi > 5$ mas, significance in parallax $\varpi/\sigma_{\varpi} > 10$, and PM vectors $-40 < \mu_{\alpha^*} < -18$ mas yr^{-1} and $-30 < \mu_{\delta} < 0$ mas yr^{-1}. The outcome of this process yielded 1356 low-mass stars and substellar members of the LCC association, including up to ∼400 BD and FFP candidates, depending on the assumed age for the group (Mejías et al. 2022a). Our selection procedure is tuned to identify only the most robust candidates, and therefore, the sample is incomplete. In particular, we worried

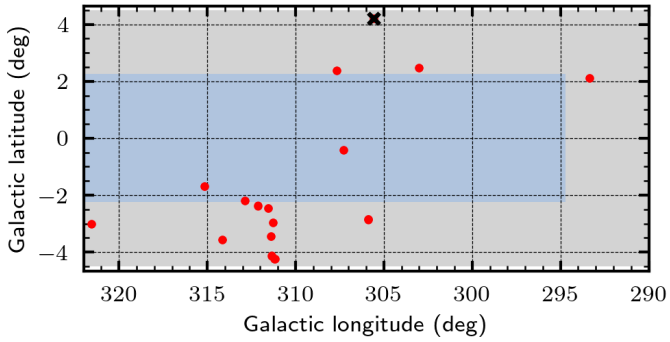

Fig. 1. Map of the Galactic plane area covered by the VVV (light blue) and VVVX (gray) surveys that overlap with the southern extension of the LCC association members (Prisinzano et al. 2022; Guo et al. 2025). The red circles show the location of the binary objects listed in Table 1. For example, VVVX-FFP-001 is the black symbol located on top at l = 305.6 deg and b = 4.2 deg.

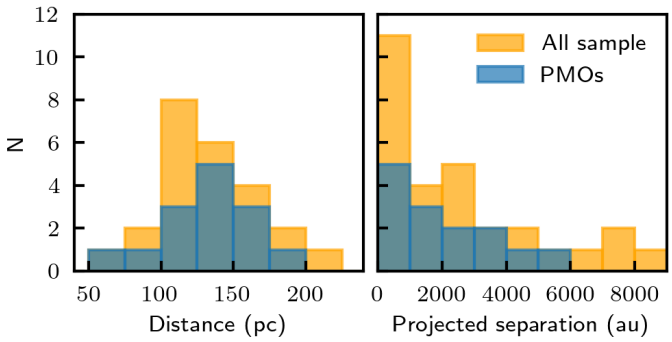

Fig. 2. Left panel: sample distance distribution in parsecs. Right panel: distribution of projected separations in au, adopting the parallax distances. While tighter systems seem to be more common, we note that this distribution appears fairly flat when plotted in logarithmic scale. In these histograms, planetary-mass objects are painted in blue, while the whole sample is in yellow.

that some fainter companions may have been culled throughout the process. Therefore, we have visually inspected the surroundings of the main targets in the VVV/X and DECaPS images, in order to search for common PM companions.

This visual search was successful, and we report here the discovery of 17 pairs of low-mass objects, a few of which are consistent with planetary masses. Furthermore, a couple of these systems appear to have additional fainter companions, that need follow up observations for confirmation. We have also included in our visual search low-mass objects listed in the binary catalog of El-Badry et al. (2021), with distances and proper motions consistent with LCC membership (i.e., VVVX-FFP-014, −015, and −016), for which we also have near-IR photometry. One of these systems, VVVX-FFP-015, is interesting because it contains a white dwarf (WD) primary candidate and could be another case of a WD+BD binary in a young region (e.g., Ferreira et al. 2024). Based on the cooling tracks of Bédard et al. (2020) and the absolute magnitude M_G, we can set a minimum time of ∼2 Myr for this WD. Unfortunately, the pre-WD phase is unconstrained in our data.

The basic parameters for the new pairs of low-mass objects are listed in Table 2. This table includes, for each pair component, the VVV/X and *Gaia* DR3 IDs, and the DR3 positions in equatorial coordinates, parallaxes and proper motions with their respective errors, the `ruwe` parameter, and optical photometry (Gaia Collaboration 2021). We also include the VVV/X near-IR photometry from Smith et al. (2018, 2025) and Alonso-García et al. (2018, 2026), respectively. The last columns of Table 1 provide the distance to the systems in pc extracted from the catalog of Bailer-Jones et al. (2021), the observed separation in arcsec, and the corresponding projected separation in au, respectively. Even though the original catalog of Mejías et al. (2022a,b) contains objects out to $\lesssim$1 kpc, we have also restricted by design the present search to nearby objects within 200 pc, where LCC membership would be more secure, and where extinction should be negligible according to the *Gaia* DR3 3D maps of Lallement et al. (2022) and Vergely et al. (2022). All but two of the secondary stars with available astrometry have `ruwe` $\leq$ 1.5, deemed to be adequate for good *Gaia* measurements (e.g., Lindegren et al. 2021). Note that this restriction in the `ruwe` would eliminate some candidates with large photocentric motions due to close-in unresolved companions. Table 1 also lists systems with poor *Gaia* astrometry for one of the components, that should be considered as low probability candidates.

3. Analysis

Figure 1 shows the locations of the binary FFPs in the Galactic coordinates map, within the VVV/X survey footprint. The candidates are widely distributed in the southern plane of the Milky Way, consistent with the distribution of the LCC association on the sky. There appears to be a slight concentration (unrelated to extinction) containing half a dozen low-mass LCC binary systems centered at $l \sim 311.5°$, $b \sim -3.0°$.

As mentioned above, Bohn et al. (2022) studied wide companions for K-type main-sequence stars in the Sco-Cen association with *Gaia*. They found 110 co-moving companions with separations between 0.6″ and 80″, corresponding to projected separations from 90 to 10^4 au. These companions exhibit a wide range of properties, including 20 companions in the BD mass regime, down to 20 $M_{\rm Jup}$. Figure 2 shows the distribution of distances in pc and projected separations in au for the sample in Table 1. This range of projected separations is similar to that found in the sample of companions of Bohn et al. (2022), and shows an extension toward closer binaries when compared with other studies (e.g., Jiménez-Esteban et al. 2019). The distribution of logarithmic projected separations is nearly uniform for our sample objects, ranging from 135 to $\sim 10^4$ au, indicating that these are very wide pairs. There is an indication that the tighter systems may be more common, but our search is insensitive to smaller separations (<1″). Clearly, the present work gives just an initial glimpse at the binary FFPs in the LCC association, and higher resolution images are needed to search for closer companions in the sample. Furthermore, our search may be missing low-mass late-type companions, too faint to be detected by *Gaia*. Such objects would be detected only in the near- or mid-IR surveys (Ivanov et al. 2013; Luhman 2014).

Figure 3 presents the observed optical G *vs.* $(G_{\rm BP} - G_{\rm RP})$ and near-IR J *vs.* $(J - K_{\rm s})$ CMDs from *Gaia* and VVV/X, respectively, along with the observed $(G_{\rm BP} - G_{\rm RP})$ *vs.* $(J - K_{\rm s})$ color-color diagram and the *Gaia* vector PM diagram. The sources show a relatively narrow color-spread in the near-IR in comparison with the wide color span (∼2.5 mag) exhibited in the optical CMD.

Figure 4 shows the optical M_G *vs* $(G_{\rm BP} - G_{\rm RP})$, $(G - G_{\rm RP})$, and near-IR M_J *vs* $(J - K_{\rm s})$ absolute CMDs from *Gaia* and VVV/X, respectively, obtained assuming the distances listed in Table 1. The M_G and M_J absolute magnitude distributions for all the sources are presented in Fig. 5, showing that we reach very faint

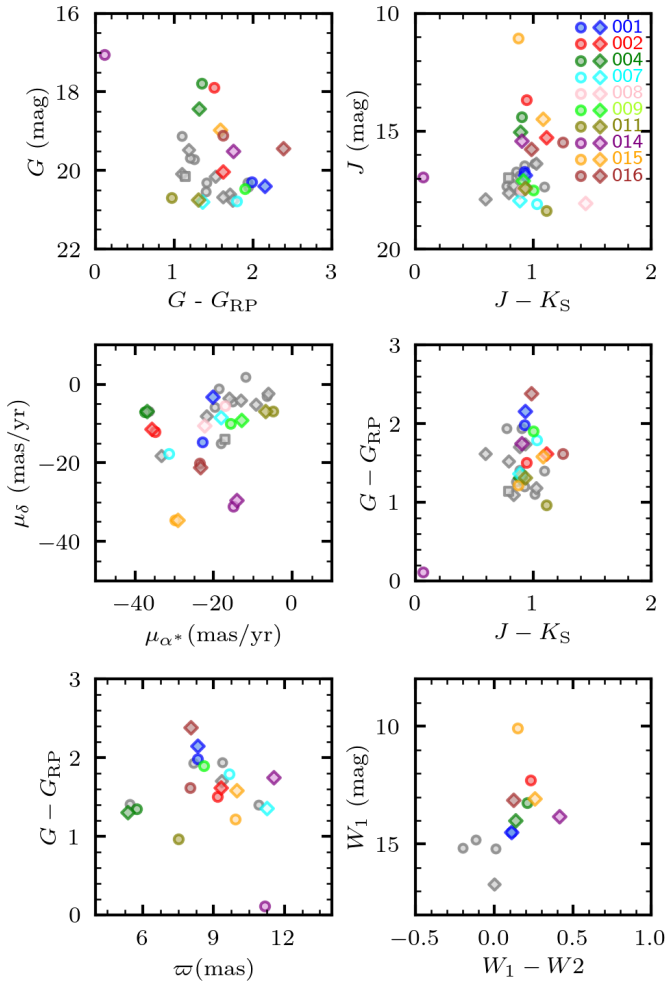

Fig. 3. Top panels: observed CMDs in the visible (left) and near-IR (right) for the sample objects from Table 1. Colored circles and diamonds represent the A and B components of each pair for which the parallax difference is consistent within parallax errors, while gray errorbars represents systems with discrepant parallaxes. Note the narrow color-spread in the near-IR CMD, compared with the wide color span exhibited by the targets in the optical CMD. Middle panels: the *Gaia* DR3 PM vector diagram (left) and visual-near-IR color-color diagram. Bottom panels: *Gaia* DR3 parallax distribution as a function of *Gaia* color index (left) and the unWISE CMD for the systems with available photometry (right).

candidates. Note that while there is some overlap in the magnitude range covered, our sample provides an extension to the sample of faint companions to the K-type main sequence stars of Bohn et al. (2022), by ∼2.5 magnitudes and, therefore, to much lower masses.

In addition, we have also examined the mid-IR photometry from the WISE satellite for the positions of our targets. In spite of being located in the Galactic plane, where extinction is severe, and confusion can be important, these relatively nearby sources may be bright enough at mid-IR wavelengths to dominate over distant background sources. Only about half of the sources were detected in the unWISE catalog using a $r < 4''$ matching radius. These sources are VVVX-FFP-001, 002, 004, 005, 006, and 011. Fig. 3 shows their mid-IR colors are relatively normal for such late-type sources (Pecaut & Mamajek 2013), clustering at $(W1 - W2) = 0.2 \pm 0.1$ mag, with a few exceptions. First, there are a couple of relatively bluer sources, VVVX-FFP-003A and -005B, with $(W1 - W2) = -0.20$ and -0.12 mag, respectively. These may be due to background contamination. Second, the reddest source that is VVVX-FFP-009B with $(W1 - W2) = 0.64 \pm 0.07$ mag. The extreme red color for this last source would be atypical of a background object, and instead, it may be due to the presence of a disk surrounding this young object. However, this is the source with the faintest unWISE magnitude and this detection needs confirmation.

The FFP masses depend on the ages because these objects fade rapidly as they cool on short timescales, and age measurements for the LCC association range from 8–10 Myr (Goldman et al. 2018) to 15–17 Myr (Pecaut & Mamajek 2016; Ratzenböck et al. 2023). We adopted the oldest of these ages to provide conservative mass estimates from interpolation of the ATMO2020 model isochrones (Phillips et al. 2020) with the absolute magnitude M_J. This calculation shows all objects fainter than $M_J = 11.2$ mag qualify as planetary candidates, with masses $M < 13\ M_{\rm Jup}$. There are 14 objects fulfilling this criterion, that we call candidate FFPs pending spectroscopic confirmation. The objects with $M_J < 11.2$ mag are very low-mass M-dwarfs or BDs which are also candidate members of the LCC association.

The magnitude differences between the two components of the pairs listed in Table 1 cover a wide range of colors in the optical and near-IR, but we notice that in a few cases, the color difference is reversed (secondaries that are bluer than the primaries in the optical appear redder than the primaries in the near-IR, and vice versa), perhaps indicating the presence of different kinds of objects. Flux reversal is observed in L-dwarf + T-dwarf pairs, and is attributed to the presence or absence of thick clouds in their atmospheres (e.g., Burgasser et al. 2013; Saumon & Marley 2008). Interestingly, objects fainter than $M_J = 11.2$ mag classified as FFPs also exhibit a wide range of colors. At one extreme, there is VVVX-FFP-008B that is the reddest secondary with $(J - K_s) = 1.44$ mag. At the other extreme is VVVX-FFP-014A, which is the bluest companion with $(J - K_s) = 0.1$ mag, about 0.9 mag bluer than its primary. Note that this cannot be a WD because the LCC sequence for these objects should be more luminous. However, we note that both of these systems were deemed to have low quality because the secondaries do not have *Gaia* astrometry. Indeed, the color-color diagram does not show a clear sequence as one would expect from the models. We argue that this is a real spread and not due to photometric errors or misclassification of the FFPs. This wide optical and near-IR color range would be important for future searches to take into account. The wide range of colors and flux reversals observed in our sample suggests that the existence and possibly absence of dust and molecular opacity is important and points to a continuity with the BD models. Perhaps, the giant FFPs can also be classified into T-type FFPs that would be predominantly cloudless, and L-type FFPs containing thick clouds in their atmospheres. However, a color inversion caused by the presence of IR excess due to a circumstellar disk around one of the components cannot be discarded in some objects.

Figure 6 shows the comparison with the masses found by Bohn et al. (2022) in their search for wide-orbit companions to K-type dwarfs that are members of the Sco-Cen association, which includes the LCC region mapped here. Our masses cover a different range that is complementary to their distribution but extending to much lower values, well within the planetary regime. However, while the completeness of Bohn et al. (2022) ranges from ∼80 to 100%, our search is not complete.

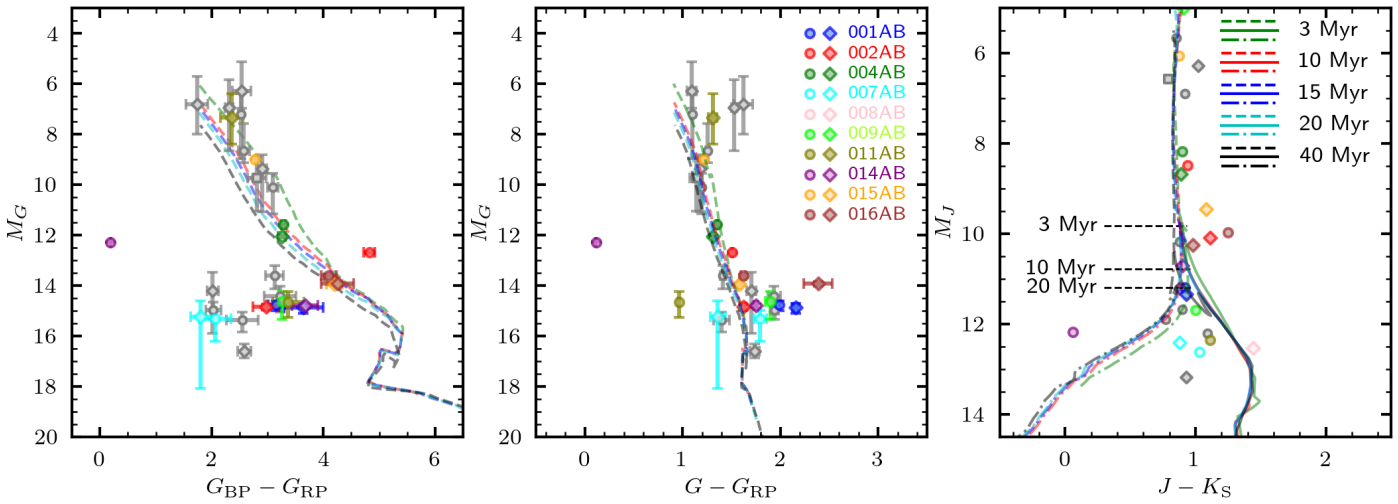

Fig. 4. Absolute CMDs in the optical and near-IR for all the sources in the sample. Colored circles and diamonds with error bars represent the A and B components, respectively, for each pair for which the parallax difference is consistent within parallax errors, while gray error bars represent systems with discrepant parallaxes. In all panels, dashed lines represent the Baraffe et al. (2015) isochrones. In the right-most panel, the solid and dot-dashed lines represent the cloudy and clear atmosphere models of Saumon & Marley (2008), respectively. The three marks at 3, 10, and 20 Myr represent the limit of 13 M_{Jup} for the associated isochrones.

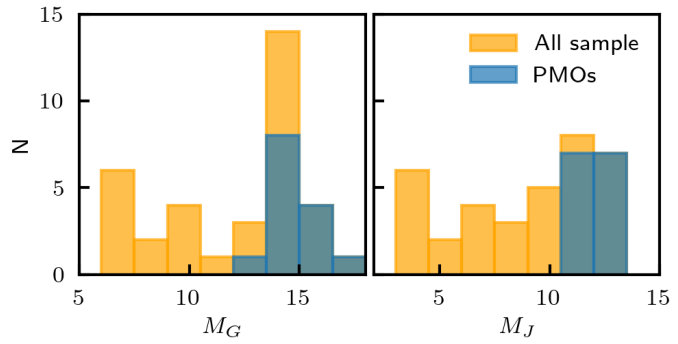

Fig. 5. Luminosity functions for all the binaries in the absolute magnitudes M_G and M_J. As discussed in the text, the rightmost bins with $M_J > 11.2$ mag in the bottom panel would be classified as FFPs using an isochrone of 17 Myr.

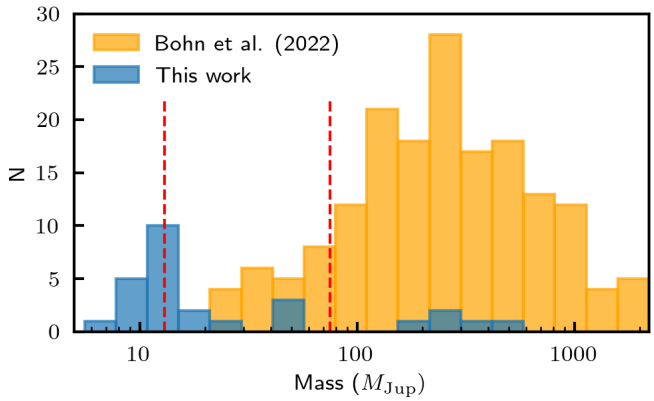

Fig. 6. Mass distribution of the binary components from our sample (blue bars) compared with the masses found by Bohn et al. (2022) in their search for low-mass companions to K-type dwarfs that are LCC members (yellow bars). The vertical red lines separate systems classified as planets (left), BDs (middle), or stars (right).

4. VVVX-FFP-001, a case study

As a case study, we describe in detail VVVX-FFP-001, the first candidate binary FFP that we discovered. It is located in the Galactic plane at equatorial coordinates (α, δ) = (13 11 49.14, −58 32 59.5), and Galactic coordinates (l, b) = (305.59509, 4.21653) deg, as listed in Table 1. The distance of 120 ± 10 pc is adopted using the *Gaia* DR3 parallax of VVVX-FFP-001A, $\varpi = 8.31 \pm 0.74$ mas yr^{-1}. The parallax of the other component is ill-determined ($\varpi = -0.99 \pm 0.89$ mas yr^{-1}), revealing a poorer astrometric solution, which would hopefully improve with subsequent *Gaia* data releases. For the *Gaia* distance, its 3D coordinates are $X = 69.6$ pc, $Y = -97.3$ pc, $Z = 8.8$ pc, assuming the Sun to be at $(X, Y, Z)_\odot = (0, 0, 0)$. The position, parallax, and PMs indicate that VVVX-FFP-001 is a member of the LCC association, located on its near side.

VVVX provides us with near-IR photometry and *Gaia* and DECaPS (Schlafly et al. 2018) with optical photometry. Figure 7 shows the optical and near-IR finding charts for VVVX-FFP-001. There are more sources in the DECaPS images than in the other surveys. Indeed, Moolekamp et al. (2019) carried out a DECAM search for low-mass stars and substellar objects with spectral types M1 to L1 in this region of the LCC association. They also found a large number of faint objects without PMs and JHK_S photometry, that were deemed to be nonmembers.

Despite its low Galactic latitude, VVVX-FFP-001 is located in a moderately low extinction field, with an average extinction along the line of sight of $A_V = 2.04$ mag, $E(B-V) = 0.66$ mag, $A_K = 0.225$ mag, $E(J-K) = 0.30$ mag (Schlafly & Finkbeiner 2011). However, because of its proximity, the total extinction of this object is much smaller than that, as confirmed by the recent *Gaia* DR3 3-D maps of Lallement et al. (2022) and Vergely et al. (2022). The total extinction at 120 pc from the EXPLORE G-TOMO 3D maps in the direction of the source (Lallement et al. 2022) is $A_V = 0.069$ mag, $A_K = 0.007$ mag, yielding $E(J-K_s) = 0.0097$ mag. In fact, the lack of reddening exhibited by this source helps to confirm its proximity, as beyond this distance there is a dust cloud in this direction, where the optical extinction jumps by about $A_V = 0.3$ mag from 125 to 200 pc.

The optical and near-IR images reveal that this is clearly a binary object, with the two components AB separated by 0.73″,

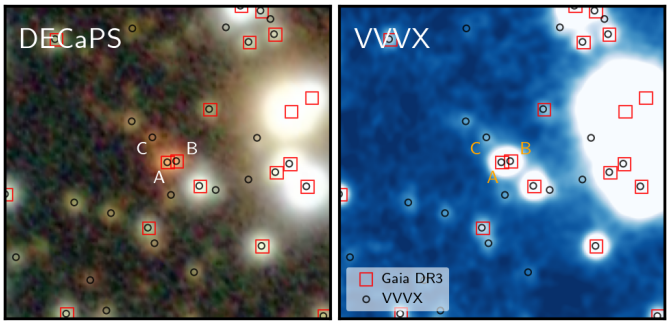

Fig. 7. Left panel: optical finding chart for VVVX-FFP-001, that is the double source located at the center of the images. These images are 25″ on a side, with north on top and east to the left. Right panel: map of the matched sources from the VVVX (blue squares) and *Gaia* DR3 (red circles) catalogs.

according to *Gaia* DR3 astrometry (Fig. 7). This small angular separation is equivalent to a projected separation of 88 au at the distance of 120 pc. We argue that this binary source is not due to a chance alignment, as the *Gaia* DR3 magnitudes and PMs are similar, and the background contamination rate should be negligible (Tian et al. 2020; El-Badry et al. 2021). In addition, we expect a similar chemical composition for both components (Hawkins et al. 2020; Nelson et al. 2021).

Table 2 lists all the optical and near-IR photometric measurements available for this object, including the absolute magnitudes assuming a distance of 120 pc. *Gaia* DR3 photometry yields $G = 20.32$ mag and $(G_{BP} - G_{RP}) = 3.16$ mag for component A, and $G = 20.42$ mag and $(G_{BP} - G_{RP}) = 3.65$ mag for component B. The magnitude difference $\Delta G = 0.10$ mag argues for an almost equal mass binary, with mass ratio $q \sim 1$. The optical color difference is larger $\Delta(G_{BP} - G_{RP}) = 0.49$ mag, with component B being fainter and redder. This color difference may be intrinsic, or it may indicate that component B has a dusty disk.

The VVVX near-IR photometry yields similar results. Component A has observed $K_s = 15.80 \pm 0.05$ mag and $(J - K_s) = 0.93$ mag, while component B has observed $K_s = 15.90 \pm 0.05$ mag and $(J - K_s) = 0.92$ mag. Again, the magnitude difference of only $\Delta K_s = 0.10$ mag argues for nearly equal masses, with component B having a slightly lower mass. The near-IR color difference is smaller than in the optical, with $\Delta(J - K_s) = 0.01$ mag. The optical-near-IR colors for both components are identical, $(G - K_s) = 4.52$ mag. Fig. 8 presents the optical and near-IR CMDs, color-color diagrams, and vector PM diagram for a 2 arcmin region centered in VVVX-FFP-001, with both binary components highlighted.

The VVVX-FFP-001 components have near-IR absolute magnitudes $M_J = 11.33$ and $M_J = 11.42$ mag, respectively. Assuming the age of the LCC association conservatively is 17 Myr, the isochrones are consistent with planetary masses for both components of VVVX-FFP-001. Using the ATMO2020 isochrones (Phillips et al. 2020), we find $M_A \sim M_B \sim 12.5$ M_{Jup} for both components.

The low mass of the components and their observed separation indicate that the binding energy is very low, $-E_{bind} = 2.6 \times 10^{40}$ erg[3], and this young system may not survive for long in the Galactic disk. Close et al. (2007) discuss the binding energy for very low mass objects. As an example, VVVX-FFP-001's binding force is smaller than the binding force of Proxima

[3] Calculated following the prescriptions of Close et al. (2007) and Burgasser et al. (2007).

Table 2. Additional photometry for VVVX-FFP-001.

Survey	Filter	VVVX-FFP-001A	VVVX-FFP-001B	VVVX-FFP-001C
VVVX	J	16.72 ± 0.02	16.86 ± 0.02	18.94 ± 0.06
VVVX	H	16.20 ± 0.03	16.21 ± 0.03	18.34 ± 0.10
VVVX	K_s	15.80 ± 0.05	15.93 ± 0.05	17.89 ± 0.28
VVVX	$(J - K_s)$	0.92 ± 0.05	0.93 ± 0.05	1.05 ± 0.28
Gaia DR3	G	20.32 ± 0.01	20.42 ± 0.01	...
Gaia DR3	$(G_{BP} - G_{RP})$	3.16 ± 0.01	3.65 ± 0.01	...
Gaia/VVVX	$(G - K_s)$	4.52 ± 0.05	4.52 ± 0.05	...
DECaPS	g	22.42 ± 0.04	22.43 ± 0.04	...
DECaPS	r	21.09 ± 0.02	21.37 ± 0.03	22.88 ± 0.10
DECaPS	i	18.99 ± 0.01	19.39 ± 0.01	21.36 ± 0.05
DECaPS	z	18.18 ± 0.01	18.50 ± 0.01	20.36 ± 0.04
DECaPS	Y	18.03 ± 0.01	18.23 ± 0.01	20.60 ± 0.06
DECaPS	$(r - i)$	2.10 ± 0.02	1.98 ± 0.03	1.52 ± 0.12
Gaia DR3	M_G	14.92 ± 0.18	15.02 ± 0.18	...
VVVX	M_J	11.32 ± 0.18	11.46 ± 0.18	13.54 ± 0.19
VVVX	M_{K_s}	10.40 ± 0.19	10.53 ± 0.19	12.49 ± 0.28

Centauri (see Kervella et al. 2017). The VVVX-FFP-001 system would then have one of the lowest binding energies known, comparable only to Oph98 (Fontanive et al. 2020). Such loosely bound systems are not expected to survive long (e.g., Close et al. 2007; Mužić et al. 2012; Fontanive et al. 2020). The study of such systems can also teach us about the Galactic tidal forces (Chaname & Gould 2004; Tian et al. 2020). We note also that in the stellar regime, Zúñiga-Fernández et al. (2021) found a higher binary fraction for the younger moving groups, and that this fraction diminishes with age. In this regard, the loose nature and youth of VVVX-FFP-001 is consistent with a continuous transition between stellar and planetary-mass systems.

There is another fainter red object nearby that might be member of the system. We call this VVVX-FFP-001 C, cautioning that this might be a background interloper. This source has $K_s = 17.89$ mag and $(J - K_s) = 1.05$ mag. It is beyond the detection limit of *Gaia*, but it can be clearly seen in the DECaPS and VVVX images (Fig. 7). The measured VVVX position is $\alpha = 197.955384$ deg, $\delta = -58.549311$ deg. The separation between components A and C is 2.0″, equivalent to 240 au at a distance of 120 pc. If this faint object belongs to the VVVX-FFP-001 system, its near-IR absolute magnitude would be $M_J = 13.54$ mag. Therefore, its mass should be much smaller than the AB components, with $M \sim 6$ M_{Jup}. Even though the chance alignment possibility is very low, and genuine triplets should not be rare (Tokovinin 2014), this should be treated only as a candidate, as there are no parallax nor PM measurements for this object.

5. Summary of other individual targets

Considering the census of individual objects, this binary sample contains 35 objects in total, including: 14 planetary-mass object candidates (PMOs), 8 BDs, 12 stars (S), and also 1 WD. These objects form 17 pairs in total, divided as follows: two PMO+PMO, three BD+BD, two S+BD, nine S+PMO, and one WD+BD. We discuss briefly the individual systems below. This is appropriate because they make up a heterogeneous sample with diverse characteristics.

VVVX-FFP-001 consists of a tight (0.7″ or 88 au projected separation) pair of identical mass FFPs with $M \sim 12$ M_{Jup} with an additional unconfirmed companion, which was discussed in

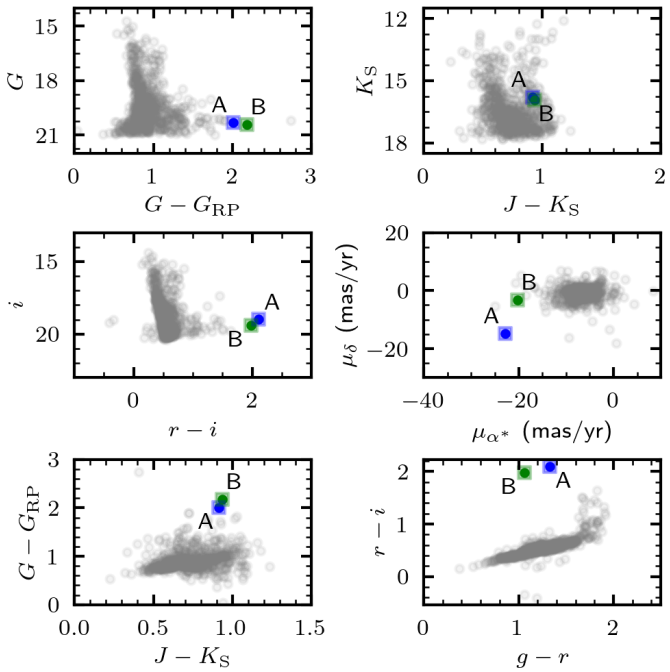

Fig. 8. Top panels: observed CMDs from *Gaia* and VVVX (from left to right) for the 2′ field region surrounding VVVX-FFP-001. The primary (A) and secondary (B) binary components are indicated. Middle panels: from left to right, the DECaPS CMD and *Gaia* vector PM diagram. Bottom panels: *Gaia*-VVVX optical-near-IR color-color diagram, and DECaPS optical color-color diagram for the same region.

the previous Section (see Table 2 and Figs. 7–8). A caveat is that the secondary has a negative parallax measured, which may be due to blending with the primary. This system is well detected by unWISE, yielding a typical color $(W1 - W2) = 0.11 \pm 0.02$ mag, although the components are unresolved.

VVVX-FFP-002 consists of two tight BDs (2.5″ or 275 au projected separation) with masses $M_A \sim 55$ M_{Jup} and $M_B \sim 15$ M_{Jup}. They have a large optical color difference $\Delta(G_{BP} - G_{RP}) = 2.0$ mag, with the primary being redder. This color difference is reversed in the near-IR, with the primary being about 0.2 mag bluer than the secondary. In fact, at optical wavelengths the primary is by far the reddest object of the whole sample, with $(G_{BP} - G_{RP}) = 4.82$ mag. This is the system with the brightest unWISE $W1$ band magnitudes, yielding a typical color $(W1 - W2) = 0.24 \pm 0.01$ mag, although the components are unresolved.

VVVX-FFP-003 consists of a pair of low mass candidate with $M_B \sim 12$ M_{Jup} and a low-mass star, separated by 12″ or 1283 au projected separation. The more massive giant planet is bluer in $(G_{BP} - G_{RP})$ and $(J - K_s)$, but redder in $(G - G_{RP})$. A caveat is that the secondary has a different PM in declination by $\sim 3\,\sigma$. The primary has an unWISE $W1$ band counterpart, with the bluest mid-IR color of the sample, $(W1 - W2) = -0.20 \pm 0.05$ mag, while the secondary is only detected in the $W2$ band.

VVVX-FFP-004 consists of a pair of BDs of estimated masses of $M \sim 55$ M_{Jup} and $M \sim 52$ M_{Jup}, separated by 13.4″ (2338 au projected separation). The primary and secondary have nearly identical optical and near-IR colors, with the primary being about 0.7 mag brighter than the BD secondary in J. Both components of this system are well detected by unWISE, with the primary component being about 1.0 mag brighter in the unWISE $W1$ band, and 0.1 mag redder in the $(W1 - W2)$ color.

VVVX-FFP-005 consists of a planetary-mass object candidate and a stellar-mass pair, with $M_B \sim 12.5$ M_{Jup}, separated by 16″ (2031 au projected separation). The two components have similar $\Delta(J - K_s)$ colors, but unfortunately, there are no *Gaia* colors available for one of the objects. Both components of this system are well detected by unWISE, though, with the primary being about 1.5 mag brighter in the unWISE $W1$ band, and 0.4 mag redder in the $(W1 - W2)$ color.

VVVX-FFP-006 is a pair consisting of a planetary-mass object and a star, with a separation of 2.1″ or projected 229 au. The mass of the secondary is $M_B \sim 11$ M_{Jup}. In all colors, the primary is bluer than the secondary component.

VVVX-FFP-007 consists of a pair of nearly equal mass FFP candidates with $M_A \sim M_B \sim 8{-}9$ M_{Jup}, separated on the sky by 50″ (5195 au projected), comprising the system with the smallest total mass. One caveat is that the secondary has different PMs by $>3\sigma$. In all reported colors, the primary is slightly redder than the secondary.

VVVX-FFP-008 consists of a giant planet with estimated mass of $M_B \sim 8{-}9$ M_{Jup}, separated by 17.1″ (1826 au projected separation) from a stellar companion. There are no optical $(G_{BP} - G_{RP})$ colors available from *Gaia* for the components of this system. However, unWISE magnitudes are available, with the secondary having a significantly redder unWISE color: $(W1 - W2)_A = 0.14 \pm 0.06$ vs $(W1 - W2)_B = 0.64 \pm 0.07$ mag.

VVVX-FFP-009 consists of a planetary-mass companion candidate with $M_B \sim 11$ M_{Jup}, at 49″ from the stellar primary. The primary is 0.16 mag bluer than the secondary in the near-IR. There are no optical $(G_{BP} - G_{RP})$ colors available from *Gaia* for the primary component of this system.

VVVX-FFP-010 represents a brown-dwarf candidate in a triple stellar-mass system. The mass of the companion is $M_B \sim 15.0$ M_{Jup}, and this object is separated 36.8″ on sky, or a projected distance of 6742 au from the closer object. They also have nearly identical near-IR colors. A caveat is that the secondary has different parallax by $>3\,\sigma$. Another caveat is that the tertiary component has different PM in declination by $>3\,\sigma$. For simplicity and to avoid confusion, only the primary and secondary are plotted in the diagrams.

VVVX-FFP-011 consists of a planetary-mass companion candidate $M_B \sim 10$ M_{Jup}, separated by 27.8″ or 3706 au projected from the primary star. The secondary object is redder both in the optical and near-IR.

VVVX-FFP-012 consists of a pair made of a star and a planetary-mass companion candidate. The giant planet candidate has a mass of $M_B \sim 10$ M_{Jup}, separated by 9.7″ from the primary (equivalent to 888 au of projected separation). The most massive giant planet is redder both in the optical and near-IR. A couple of caveats are that the primary has `ruwe` ~2.0, and that the secondary has different parallax by $>3\,\sigma$.

VVVX-FFP-013 also consists of a planetary-mass companion candidate in a tight (1.6″ or 196 au projected separation) pair with a stellar object, with $M_B \sim 11$ M_{Jup}. The planet candidate is redder both in the optical and near-IR, with a sizable color difference $\Delta(G_{BP} - G_{RP}) = 0.9$ mag and $\Delta(J - K_s) = 0.1$ mag. A caveat is that the secondary has different parallax by $>3\,\sigma$.

VVVX-FFP-014 consists of a WD plus a BD located very close to the BD–giant planet boundary, with $M_B \sim 12{-}14$ M_{Jup}. The components are separated by 14″ (or a projected distance of 1237 au). This system was classified as a WD-M-dwarf binary by El-Badry et al. (2021).

VVVX-FFP-015 consists of an M-dwarf with a BD companion of estimated mass $M_B \sim 30$ M_{Jup}, separated by 5.6″ or 561 au projected. The primary star is bluer than the secondary

in both the optical and near-IR. There is a third faint object that may be another component, but it needs confirmation because it lacks *Gaia* astrometry. This system was classified as an M-dwarf binary by El-Badry et al. (2021).

VVVX-FFP-016 is a pair of very red BDs, with masses of $M_A \sim M_B \sim 15-16\ M_{Jup}$ and separated 1.7″ or a projected distance of 213 au. They have similar optical colors, but the primary is 0.25 mag redder in the near-IR. This system was also classified as a M-dwarf binary by El-Badry et al. (2021).

VVVX-FFP-017 is a pair consisting of a planetary-mass companion candidate and a stellar candidate host, separated on sky by 41.1″ (2540 au projected). The giant planet has an estimated mass of $M_B \sim 7-8\ M_{Jup}$. A couple of caveats are that the primary has different parallax by $>3\sigma$, and that the secondary has different PM in declination by about 4σ.

6. Discussion

We have to consider alternative interpretations other than a binary FFP for the systems reported here.

6.1. Contamination

In general, at low Galactic latitudes, it is difficult to discard the background contamination, so we must also consider the possibility that some of the systems could be distant galaxies. Numerous background galaxies can be appreciated in the deep near-IR images of the VVV survey (Baravalle et al. 2021). However, the significant parallaxes and PMs of the objects and their point-source appearance indicate these objects are not galaxies. A similar argument holds for QSOs, which may appear as point sources in the near-IR images but whose parallaxes and proper motions readily separate them from the closer-in populations in LCC.

Red objects can also be background giants or dwarf stars from the disk. A giant star can be easily discarded because at these faint magnitudes ($K_s = 15.8$ mag) this giant would be very distant, far beyond the Milky Way disk. For example, a red clump giant yields a distance of 30 kpc. While there are halo giants at these large distances, the measured PM would give an unreasonably large tangential velocity for membership in the Milky Way. Red main-sequence stars at ∼120 pc should be brighter than the observations indicate, so one possibility is that the parallaxes are erroneous and the objects are more distant. However, a more distant late M-dwarf or BD would be inconsistent with the optical and near-IR photometry. If the distance is larger than ∼200 pc (which could be the case of the 7 targets with discrepant parallaxes), then the extinction and reddening become too high: $A_V > 0.3$ mag, $A_K > 0.033$ mag, $E(J-K_s) > 0.045$ mag to be consistent with the observed colors. Therefore, we consider the scenario of a late M-dwarf or BD to be unlikely given the position, distance, and PMs, which are consistent with the LCC association. Hopefully the future *Gaia* data releases would improve the parallax measurement.

6.2. Classification

The objects studied here comprise a heterogeneous sample. Substellar and planetary-mass objects show a wide range of colors, especially in the optical wavelengths. This color spread is real and cannot be accounted for by photometric errors or object misclassification in all cases. Riello et al. (2021) have shown an issue with the G_{BP} photometry at the very faint magnitude limit, which may imply an overestimation of the flux in the BP band for the faint sources presented here. However, this range of colors is also present in the much less affected $(G - G_{RP})$ color. The optical and near-IR color-magnitude diagrams in Fig. 4 show most of the candidates lie at the region where low-mass substellar and planetary-mass objects are expected, for ages younger than 40 Myr. A similar wide range of colors is observed for field BDs, which are classified according to the presence or absence of clouds in the atmosphere into L- and T-types, respectively, and it seems these young FFPs may be sharing these properties. Furthermore, big spectral differences of giant exoplanet atmospheres due to clouds are predicted by the models at optical and IR wavelengths (e.g., Marley et al. 1999; Burrows et al. 2000; Sudarsky et al. 2000, 2003). Both components of a binary are located at the same distance and share the same chemical composition and age. Also, some pairs share common proper motions, have consistent parallaxes, and even have similar masses as estimated from the J band absolute magnitudes, yet the components show different colors, indicating a real difference in their intrinsic properties.

6.3. Formation scenario

The discovery of these binary FFPs will help to test theories of binary star and planet formation. Miret-Roig et al. (2022) argue that core-collapse models' predictions fall short in explaining the current population of young FFPs, and that a large number of objects must form in the disk of a host star, being subsequently expelled by dynamical interactions. However, Veras & Raymond (2012) argued from N-body simulations that planet-planet scattering alone cannot explain the population of all FFPs. The high observed abundance of FFPs suggests that different formation mechanisms are required. Therefore, it is important to build planet samples formed by core collapse, with well-understood completeness, to compare with those of planets ejected from circumstellar disks.

Moreover, Ma et al. (2016) found that microlensing predictions for FFPs provide a higher number of event rates and longer median timescales than those observed by Sumi et al. (2011). They argued that the excess of short-timescale microlensing events is too large to be reconciled with the core accretion theory or the gravitational instability models. While other authors found a smaller fraction of short-timescale microlensing events (e.g., Mroz et al. 2017), a couple of facts appear interesting: the ejection process contributes to the frequency of FFPs, and there may be more FFPs than planets bound to their parent stars (e.g., Gould et al. 2022).

Interestingly, the binaries composed only of FFPs and BDs in this sample are similar to AB Pic b and to β Pic b both in age and mass (Chauvin et al. 2005; Lagrange et al. 2010, 2018), but probably formed differently: we argue that the low-mass binary objects are orphan planets, that did not form in a disk around a normal star and were then ejected by dynamical processes. It is unlikely to eject simultaneously two objects in the same direction that would remain bound to each other, as a minute velocity difference of only a couple of km s^{-1} at the time of ejection would lead to a separation of millions of au after a few million years, contrary to the relatively small binary separations observed. In view of the existence of these candidate binary objects in LCC, it seems unlikely to expect that all FFPs formed from ejections due to dynamical instabilities in forming planetary systems. This favors the gravitational collapse formation mechanism for at least a fraction of the FFP population, showing a continuity with the formation process of normal stars down to these lowest mass objects.

6.4. Population

It is also interesting that so far only single FFPs have been detected using microlensing (Sumi et al. 2011; Gould et al. 2022, and references therein). The present work suggests that microlensing by binary FFPs should also be detectable, and we argue that the frequency of these binary events may not be negligible. In fact, current microlensing events by binary FFPs may have been discarded simply because their timescales would be too different and would not fit a single microlensing light curve. Interestingly, Sajadian (2025) have determined the yield for binary FFPs in the Roman Galactic Exoplanet Survey (RGES) to be $\lesssim$50 giant planets (and a few Earth-mass binary systems). We note that for large microlensing event samples, there are similar samples of forsaken objects (Navarro et al. 2020) that are discarded because they do not fulfill all the requirements for the single microlensing light curve fit. A wide variety of light curves are expected: systems such as the ones discovered here would look like a couple of isolated short timescale events repeated after a very long time, while tighter binary FFP systems would exhibit very complex microlensing light curves. Therefore, we advocate that the reexamination of the rejected microlensing light curves may be profitable, as this may reveal very interesting binary FFPs, and may also provide additional statistically meaningful constraints on the frequency of these objects.

The observed trend for the close-in FFP binary systems to be more common (Fig. 2) would be interesting also in the context of astrobiology. In the absence of a parent star that ablates its surface, the FFPs may be prone to maintaining extended atmospheres. In fact, FFPs may also be water-rich, containing vast liquid oceans that may be common sites of life (Stevenson 1999; Avila et al. 2021). The tight binary FFPs in particular would be tidally heated, providing a long-term energy source to keep water oceans in a liquid state. In the presence of other energy sources like volcanism, these may be suitable environments where life can develop, and that could be stable enough to provide long-term habitats. In fact, we cannot discard the possibility that the nearest inhabited world may be a (yet to be discovered) tight binary FFP in the solar vicinity. Even though these nearby tight binary FFPs would be exceedingly elusive to discover, gravitational microlensing seems to be the most promising technique for distant objects and future mid-IR all-sky space-based surveys for the closer ones.

Despite the recent progress in the detection of FFPs and the findings of binary FFPs in young stellar associations, the fraction of binary objects remains mostly unconstrained. For instance, Todorov et al. (2014) found the binary fraction of cool objects (i.e., SpT > M6) is ~4% at separations >10 pc in Taurus and Chamaeleon, indicating disruption after $\gtrsim$10 Myr. Bouy et al. (2022) found one likely binary object in the sample of Miret-Roig et al. (2022), while more recent studies using JWST and Euclid in young regions have found small binary fractions of $\lesssim$1% among FFPs (e.g., Bouy et al. 2025; Luhman et al. 2024; Langeveld et al. 2024; De Furio et al. 2025). The largest fraction of FFPs is reported by Pearson & McCaughrean (2023), but their 9% of binaries is controversial as Luhman et al. (2024) and Luhman (2025) have reported that most of their candidate binaries lacking astrometric solutions are actually background sources. Our findings reveal the binary fraction of BDs and FFPs in LCC might be $\gtrsim$2%, in line with the current literature values. However, we are still under the low-number statistics regime and, more data is urgently needed to elucidate the actual presence of single and binary FFPs in young nearby stellar associations.

Finally, we would like to underline that we loosely call the target sample binary FFPs. While all of these systems might have been formed as real bound binaries, some of them might already be unbound or are presently becoming unbound. It is reasonable to expect that not all of them will remain bound due to their low binding energy that cannot compete with the Galactic tidal field or close stellar encounters. Therefore, a few of the ones with large separations (of several thousand au like VVVX-FFP-007 for instance) may already be mere common PM pairs free floating in the Galactic potential, but they nonetheless had a -likely- binary or triple origin. In fact, Elliott & Bayo (2016) argue that there is a preference for wide systems to have more than two components, suggesting that the majority of wide binaries in young groups are primordial. It is clear that the present discoveries are just beginning to probe the transition region between bound and unbound binary-triple systems of very low mass (composed of BD or giant planets) in the LCC association.

7. Conclusions

We have reported 17 young low-mass candidate binaries in the nearby LCC association. A couple of these candidates have additional faint companions that need confirmation to secure them as triple systems. Adopting an age of 17 Myr for the LCC association, we deem that 14 of the components are candidate giant FFPs because they are fainter than $M_J \lesssim 11.2$ mag or 13 $M_{\rm Jup}$. These FFP binary systems might represent $\gtrsim$2% of the population of FFPs and BDs in the LCC association. Another interesting result is that these young FFPs exhibit a wide range of optical and near-IR colors. The wide color ranges and flux reversal are akin to those found in BDs due to the presence or absence of clouds, suggesting that these giant FFPs have similar properties as those of BDs. This would be something to consider for modeling giant FFPs and for future FFP searches.

The mere existence of these binary objects suggests that not all FFPs originate from ejections due to dynamical instabilities in forming planetary systems. We argue that it is likely that binary FFP systems like VVVX-FFP-001 or -007 have formed by gravitational core collapse. The tighter system discovered here is VVVX-FFP-001 with a projected separation of 88 au. The rest of the systems have wider projected separations up to 6 742 au, and several may not remain bound for long. This work also suggests that microlensing by binary FFPs should be detectable, and that their frequency may not be negligible.

The present discoveries confirm that binary FFPs may be common and not rare exceptions, and we are probing the transition region between bound and unbound systems. This opens up some new avenues for observational and theoretical research such as, for instance, the actual frequency and the main formation mechanism of binary FFPs, the fraction of these binaries that will remain bound after the effects of the Galactic tidal field and stellar collisions, or the similarities and differences of FFPs with the bound systems that were born in disks around a host star. Follow-up spectroscopic observations are needed to characterize some benchmark objects that can, in turn, be used to plan future searches. The identification of benchmark FFPs is important to constrain the chemistry and physics of clouds and dust condensation in the models. Our work provides a prime sample for follow-up with James Webb space telescope observations, both imaging with NIRCam and MIRI to refine the PMs and search for additional companions, and spectroscopy with NIRISS and NIRSPEC to measure the compositions and kinematics. Another implication of this work is that the Roman

Galactic Plane Survey would be able to uncover thousands of new binary FFPs in LCC and the great Scorpius association. Such a survey, reaching deeper magnitudes than the VVVX in the near-IR, has the potential to discover planets with masses much smaller than Jupiter.

Data availability

The Table 1 is available at the CDS via https://cdsarc.cds.unistra.fr/viz-bin/cat/J/A+A/708/A378.

Acknowledgements. C.C. acknowledges support by ANID BASAL project FB210003. D.M. gratefully acknowledges support by the ANID BASAL projects ACE210002 and FB210003, and by Fondecyt Project No. 1220724. J.A.-G. acknowledges support from Fondecyt Regular 1201490, and ANID – Millennium Science Initiative Program – ICN12_009 awarded to the Millennium Institute of Astrophysics MAS. R.K.S. acknowledges support from CNPq/Brazil through projects 308298/2022-5 and 421034/2023-8. E.S. acknowledges support by MCIN/AEI/10.13039/501100011033/ through grant PID2020-112949GB-I00. We gratefully acknowledge the use of data from the ESO Public Survey program IDs 179.B-2002 and 198.B-2004 taken with the VISTA telescope and data products from the Cambridge Astronomical Survey Unit. This work has made use of data from the European Space Agency (ESA) mission *Gaia* (https://www.cosmos.esa.int/gaia), processed by the *Gaia* Data Processing and Analysis Consortium (DPAC, https://www.cosmos.esa.int/web/gaia/dpac/consortium). Funding for the DPAC has been provided by national institutions, in particular the institutions participating in the *Gaia* Multilateral Agreement. This publication makes use of data products from the Two Micron All Sky Survey, which is a joint project of the University of Massachusetts and the Infrared Processing and Analysis Center/California Institute of Technology, funded by the National Aeronautics and Space Administration and the National Science Foundation. We also acknowledge use of materials developed by the EXPLORE project funded by the European Union's Horizon 2020 research and innovation programme No. 101004214.

References

Avila, P. J., Grassi T., Bovino, S., et al. 2021, Int. J. Astrobiol., 20, 300
Alonso-García, J., Saito, R. K., Hempel, M., et al. 2018, A&A, 619, A4
Alonso-García, J., Hempel, M., Saito, R., et al. 2026, A&A, 706, A301
Bailer-Jones, C., Rybizki, J., Fouesneau, M., et al. 2021, AJ, 161, 147
Baraffe, I., Homeier, D., Allard, F., et al. 2015, A&A 577, A42
Baravalle, L. D., Alonso, M. V., Minniti, D., et al. 2021, MNRAS, 502, 601
Beamín, J. C., Minniti, D., Gromadzki, M., et al. 2013, A&A, 557, L8
Bédard, A., Bergeron, B., Brassard, P., et al. 2020, ApJ, 901, 93
Best, W. M. J., Liu, M. C., Dupuy, T., et al. 2017, ApJ, 843, L4
Bohn, A., Ginski, C., Kenworthy, M. A., et al. 2022, A&A, 657, A53
Bouy, H., Tamura, M., Barrado, D., et al. 2022, A&A, 664, A111
Bouy, H, Martin, E. L., Cuillandre, J. C., et al. 2025, A&A, 696, A80
Brown, W. R. 2015, ARA&A, 53, 15
Burgasser, A. J., Reid, I. N., Siegler, N., et al. 2007, Protostars and Planets V, eds. B. Reipurth, D. Jewitt, & K. Keil (Tucson: University of Arizona Press), 951, 427
Burgasser, A. J., Sheppard, S. S., & Luhman, K. L. 2013, ApJ, 772, 129
Burrows, A., Guillot, T., Hubbard, W. B., et al. 2000, ApJ, 534, L97
Chaname, J., & Gould, A. 2004, ApJ, 601, 289
Chauvin, G., Lagrange, A.-M., Zuckerman, B., et al. 2005, A&A, 438, L29
Clanton, C., & Gaudi, B. S. 2017, ApJ, 834, 46
Close, L. M., Laird, M., Zuckerman, B., et al. 2007, ApJ, 660, 1492
Contreras-Ramos, R., Zoccali, M., Rojas, F., et al. 2017, A&A, 608, 140
De Furio, M., Meyer, M. R., Greene, T., et al. 2025, ApJ, 981, L34
de Zeeuw, P. T., Hoogerwerf, R., de Bruijne, J. H. J., Brown, A. G. A., & Blaauw, A. 1999, AJ, 117, 354
El-Badry, K., Rix, H.-W., & Heintz, T. M. 2021, MNRAS, 506, 2269
Elliott, P., Bayo, A. 2016, MNRAS, 459, 4499
Ferreira, T., Saito, R., Minniti, D., et al. 2024, MNRAS, 527, 10737
Fontanive, C., Allers, K. N., Pantoja, B., et al. 2020, ApJ, 905, L14
Gaia Collaboration (Brown, A. G. A., et al.) 2021, A&A, 649, A1
Gaia Collaboration (Vallenari, A., et al.) 2023, A&A, 674, A1
Goldman, B., Röser, S., Schilbach, E., et al. 2018, ApJ, 868, 32
Gould, A., Jung, Y. K., Hwang, K.-H., et al. 2022, JKAS, 1, 99
Guo, D., Kaper, L., Brown, A. G. A., et al. 2025, A&A, 696, A119
Hawkins, K., Lucey, M., Ting, Y. S., et al. 2020, MNRAS, 492, 1164
Ivanov, V. D., Minniti, D., Hempel, M., et al. 2013, A&A, 560, A21
Jayawardhana, R., & Ivanov, V. D. 2006, Science, 313, 1279
Jiménez-Esteban, F., Solano, E., & Rodrigo, C. 2019, AJ, 157, 78
Kervella, P., Thévenin, F., Lovis, C., et al. 2017, A&A, 598, L7
Kurtev, R., Gromadzki, M., & Beamín, J. C., 2017, MNRAS, 464, 1247
Lagrange, A.-M., Bonnefoy, M., Chauvin, G., et al. 2010, Science, 329, 57
Lagrange, A.-M., Keppler, M., Meunier, N., et al. 2018, A&A, 612, A108
Lallement, R., Vergely, J. L., Babusiaux, C., et al. 2022, A&A, 661, A147
Langeveld, A., Scholz, A., Mužić, et al. 2024, AJ, 168, 179
Lindegren, L., Klioner, S. A., Hernández, J., et al. 2021, A&A, 649, A2
Luhman, K. L. 2014, ApJ, 786, L18
Luhman, K. L. 2024, AJ, 168, 230
Luhman, K. L. 2025, MNRAS, 542L, 126
Luhman, K. L., & Esplin, T. L. 2020, AJ, 160, 44
Ma, S., Mao, S., Ida, S., et al. 2016, MNRAS, 461, L107
Marley, M. S., Gelino, C., Stephens, D., et al. 1999, ApJ, 513, 879
Mejías, A. 2022a, M Dwarfs in The VVVX Survey: A Census of Low Mass Stars, Brown Dwarfs and Free Floating Planets in The Southern Galactic Plane; Doctoral dissertation, Universidad Andrés Bello, Santiago, Chile
Mejías, A., Soto, P., Minniti, D., et al. 2022b, cosp, 44, 591
Mejías, A., Minniti, D., Alonso-García, J., et al. 2022c, A&A, 660, A131
Minniti, D., Lucas, P. W., Emerson, J. P., et al. 2010, New Astron., 15, 433
Minniti, D. 2018, ASSP, 51, 63
Miret-Roig, N., Bouy, H., Raymond, S., et al. 2022, Nat. Astron., 6, 89
Moolekamp, F. E., Mamajek, E., James, E. J., et al. 2019, MNRAS, 484, 5049
Mroz, P., Udalsky, A., Skowron, J., et al. 2017, Nature, 548, 183
Mužić, K., Radigan, J., Jayawardhana, R., et al. 2012, AJ, 144, 180
Navarro, M. G., Contreras Ramos, R., Minniti, D., et al. 2020, ApJ, 893, 65
Nelson, T., Ting, Y.-S., Hawkins, K., et al. 2021, ApJ, 921, 118
Parker, R. J., Goodwin, S. P., & Diamond, J. L. 2025, MNRAS, 540, L104
Pearson, S. G., & McCaughrean, M. J. 2023, arXiv e-prints [arXiv:2310.01231]
Pecaut, M. J., & Mamajek, E. E. 2013, ApJS, 208, 9
Pecaut, M. J., & Mamajek, E. E. 2016, MNRAS, 461, 794
Penny, M. T., Gaudi, B. S., Kerins, E., et al. 2019, ApJ, 241, 3
Phillips, M. W., Tremblin, P., Baraffe, I., et al. 2020, A&A, 637, A38
Portegies, S., & Hochart, E. 2025, Nat. Astron., 9, 957
Prisinzano, L., Damiani, F., & Sciortino, S. 2022, A&A, 664, A175
Ratzenböck, S., Grosschedl, J. E, Alves, J., et al. 2023, A&A, 678, A71
Reylé, C., Jardine, K., Fouqué, P., et al. 2021, A&A, 650, A201
Riello, M., De Angeli, F., Evans, D. W., et al. 2021, A&A, 649, A3
Rojas-Ayala, B., Iglesias, D., Minniti, D., et al. 2014, A&A, 571, A36
Saito, R., Hempel, M., Alonso-García, J., et al. 2024, A&A, 689, A148
Sajadian, S. 2025, MNRAS, 544, 1981
Saumon, D., & Marley, M.S. 2008, ApJ, 689, 1327
Schlafly, E., & Finkbeiner, D. P. 2011, ApJ, 737, 103
Schlafly, E., Green, G. M., Lang, D., et al. 2018, ApJS, 234, 39
Smith, L. C., Lucas, P. W., Contreras Peña, C., et al. 2015, MNRAS, 454, 4476
Smith, L. C., Lucas, P. W., Kurtev, R., et al. 2018, MNRAS, 474, 1826
Smith, L. C., Lucas, P. W., Koposov, S., et al. 2025, MNRAS, 536, 3707
Squicciarini, B., & Bonavita, M. 2022, A&A 666, A15
Stevenson, D. J. 1999, Nature, 400, 32
Sudarsky, D., Burrows, A., & Pinto, P. 2000, ApJ, 538, 885
Sudarsky, D., Burrows, A., & Hubeny, I. 2003, ApJ, 588, 1121
Sumi T., et al. 2011, Nature, 473, 34
Tian, H.-J., El-Badry, K., Rix, H.-W., & Gould, A. 2020, ApJS, 246, 4
Todorov, K.O., Luhman, K. L., & Konopacky, Q. M. 2014, ApJ, 778, 40
Tokovinin, A. 2014, AJ, 147, 87
Veras, D., & Raymond, S. N. 2012, MNRAS, 421, L117
Vergely, J. L., Lallement, R., & Cox, N. L. J. 2022, A&A, 664, A174
Wright, E. L., Mainzer, A., Kirkpatrick, J. D., et al. 2014, ApJ, 148, 82
Zúñiga-Fernández, S., Bayo, A., Elliott, P., et al. 2021, A&A 645, A30

Appendix A: Additional photometry

Table A.1. Additional photometry for all candidates.

VVVX ID	J	K_S	$J-K_S$	G	$G_{Bp}-G_{Rp}$	$G-K_S$	g	r	i	z	Y	$r-i$	M_G	M_J	M_{K_S}
001A	16.7	15.8	0.9	20.3	3.2	4.5	22.4	21.1	19.0	18.2	18.0	2.1	14.8	11.2	10.3
001B	16.9	15.9	0.9	20.4	3.6	4.5	22.4	21.4	19.4	18.5	18.2	2.0	14.9	11.3	10.4
002A	13.7	12.7	0.9	17.9	4.8	5.2	21.3	19.5	16.9	15.6	15.2	2.6	12.7	8.5	7.5
002B	15.3	14.2	1.1	20.0	3.0	5.9	23.9	21.9	19.1	17.5	17.0	2.7	14.9	10.1	9.0
003A	16.4	17.5	1.0	19.1	2.5	1.6	20.9	19.3	18.2	17.8	17.6	1.1	7.2	4.5	3.5
003B	17.6	16.5	0.9	20.6	2.0	4.1	21.4	20.1	19.6	19.3	19.2	0.4	14.2	11.2	10.2
004A	14.4	14.1	0.9	17.8	3.3	3.7	20.1	18.5	16.8	16.0	15.7	1.7	11.6	8.2	7.2
004B	15.0	13.5	0.9	18.4	3.3	5.0	20.8	19.1	17.4	16.6	16.3	1.7	12.1	8.7	7.8
005A	16.7	16.2	0.8	19.7	2.6	3.5	22.4	20.9	19.7	19.2	19.0	1.2	8.7	5.7	4.4
005B	17.5	16.5	0.8	20.8	⋯	4.3	21.7	20.2	18.8	18.1	17.9	1.4	14.7	11.3	10.3
006A	17.3	16.4	0.8	20.4	2.0	4.0	21.8	20.3	19.7	19.6	19.1	0.6	15.0	11.9	10.9
006B	17.9	18.5	0.6	20.7	1.7	20.7	21.5	20.0	19.2	18.7	18.5	0.8	6.8	4.0	⋯
007A	18.1	17.3	1.0	20.8	2.1	3.5	22.1	20.7	20.0	19.5	19.3	0.7	15.3	12.6	11.8
007B	17.9	17.1	0.9	20.8	1.8	3.7	22.2	20.8	20.2	19.7	19.5	0.6	15.3	12.4	11.4
008A	17.5	16.7	0.9	20.8	⋯	4.1	⋯	21.4	19.8	19.0	18.8	1.6	7.1	3.8	2.9
008B	18.1	17.2	1.4	20.9	⋯	3.6	21.6	20.3	19.7	19.4	19.2	0.5	15.3	12.5	11.7
009A	17.5	16.6	1.0	20.5	3.3	3.9	22.7	20.8	19.3	19.1	18.8	1.5	14.6	11.7	10.8
009B	17.1	16.4	0.9	20.7	⋯	4.4	22.2	20.5	19.7	19.1	18.9	0.8	8.6	5.0	4.2
010A	16.9	15.9	0.9	20.3	3.1	4.4	22.5	20.8	19.2	18.4	18.2	1.6	13.6	10.2	9.2
010B	17.3	16.3	0.8	20.1	2.5	3.8	22.0	20.3	19.2	18.7	18.6	1.1	6.3	3.5	2.5
010C	17.0	16.1	0.8	20.1	2.8	4.1	22.3	20.7	19.2	18.5	18.3	1.5	9.7	6.6	5.7
011A	18.4	17.4	1.1	20.7	3.4	3.3	23.0	21.5	19.7	18.9	18.7	1.8	14.7	12.4	11.3
011B	17.4	16.5	0.9	20.7	2.4	4.3	22.3	20.7	20.0	19.5	19.4	0.7	7.3	4.0	3.1
012A	17.4	16.4	1.1	20.5	2.5	4.1	21.6	19.9	18.5	17.8	17.6	1.4	15.4	12.2	11.3
012B	16.4	15.3	1.0	19.5	2.9	4.1	21.6	19.9	18.5	17.8	17.6	1.4	9.4	6.3	5.3
013A	17.6	16.5	0.9	20.3	3.2	3.8	21.7	20.1	19.4	19.0	18.8	0.7	14.4	11.7	10.6
013B	17.6	16.9	0.8	20.1	2.3	3.2	22.1	20.4	19.6	19.1	18.9	0.8	6.9	4.4	3.6
014A	16.9	16.9	0.1	17.0	0.2	0.2	17.1	17.1	17.2	17.4	17.5	-0.1	12.3	12.2	12.1
014B	15.4	16.7	0.9	19.5	3.7	2.8	23.3	21.5	18.4	17.3	16.9	3.0	14.8	10.7	9.8
015A	11.1	10.2	0.9	14.0	2.8	3.8	15.9	14.5	⋯	⋯	⋯	14.5	9.0	6.1	5.2
015B	14.5	13.4	1.1	19.0	4.2	5.6	22.7	20.8	18.0	16.6	16.1	2.8	14.0	9.5	8.4
016A	15.5	14.2	1.2	19.1	4.1	4.9	22.2	20.5	18.0	17.0	16.6	2.5	13.6	10.0	8.7
016B	15.8	14.8	1.0	19.4	4.3	4.7	22.5	20.8	18.4	17.4	17.1	2.3	13.9	10.2	9.3
017A	16.5	15.5	0.9	19.7	3.1	4.2	21.8	20.2	18.7	18.0	17.8	1.5	10.1	6.9	5.9
017B	17.4	16.5	0.9	20.8	2.6	4.3	22.9	21.2	19.6	18.9	18.7	1.5	16.6	13.2	12.3